Journal of Solid State Chemistry **142,** 336–343 (1999)
Article ID jssc.1998.8042, available online at http://www.idealibrary.com on IDEAL®

Tungsten Bronze-Type Solid Solutions $Ba_{6-3x}Sm_{8+2x}Ti_{18}O_{54}$ ($x = 0.3, 0.5, 0.67, 0.71$) with Superstructure

H. Okudera,[1] H. Nakamura, H. Toraya, and H. Ohsato*

Ceramics Research Laboratory, Nagoya Institute of Technology, Asahigaoka 10-6-29, Tajimi 507-0071, Japan;
**Department of Materials Science and Engineering, Nagoya Institute of Technology, Gokiso-cho, Showa-ku, Nagoya 466-8555, Japan*

Received May 27, 1998; accepted September 14, 1998

Structural parameters of tungsten bronze-type compounds $Ba_{6-3x}Sm_{8+2x}Ti_{18}O_{54}$ ($x = 0.3$, 0.5, 0.67, and 0.71) were refined in a space group *Pbnm* by the Rietveld method using high-resolution synchrotron radiation powder diffraction data. All the specimens crystallized in the orthorhombic system with a superstructure having the doubled *c* axis of the reported orthorhombic tungsten bronze-type structure. Unit-cell parameters (in Å) are $a = 12.1715(5)$, $b = 22.3772(3)$, $c = 7.67523(9)$ for $x = 0.3$, $a = 12.1568(1)$, $b = 22.3253(2)$, $c = 7.66301(7)$ for $x = 0.5$, $a = 12.1472(1)$, $b = 22.2972(2)$, $c = 7.65338(6)$ for $x = 0.67$, and $a = 12.1452(1)$, $b = 22.3029(2)$, $c = 7.65007(6)$ for $x = 0.71$, and $Z = 2$. The use of two wavelengths allowed the determination of cation and vacancy distributions over two pentagonal and five tetragonal tunnels in the structure. In the compounds with $x = 0.3$ and 0.5, pentagonal tunnel sites were fully occupied by Ba, and the remaining Ba partially substituted Sm at two of five tetragonal tunnel sites. No evidence was found for the substitution of Sm for Ba at the pentagonal sites, and thus vacancies were formed at the pentagonal sites for $x = 0.71$. An amplitude of periodic modulation along the *c* axis, which caused superstructure, was increased with increasing *x* in the compositional range examined. A relationship between observed and calculated intensities of superstructure reflections suggests the presence of local lattice distortion, which takes its minimum at $x = 0.67$.
© 1999 Academic Press

INTRODUCTION

Physical properties of $Ba_{6-3x}R_{8+2x}Ti_{18}O_{54}$ (R = La, Nd, and Sm) series have been investigated for their device applications related to their excellent dielectric properties (1–4). Matveeva *et al.* (1) reported that $Ba_{3.75}Pr_{9.5}Ti_{18}O_{54}$ ($x = 0.75$) crystallized in an orthorhombic system. Although the presence of a superstructure doubling the *c* axis was found, they refined structural parameters by assuming an average cell with a noncentrosymmetric space group *Pba*2 (No. 32). On the other hand, Ohsato *et al.* (2) confirmed the formation of solid solutions for R = Sm over the composition range $0.3 \leq x \leq 0.7$ and refined the structural parameters in a centrosymmetric space group *Pbam* (No. 55). The basic structure, assumed in these refinements, is a tungsten bronze-type framework structure formed by TiO_6 octahedra sharing all apices with each other, and is characterized by distorted tetragonal and pentagonal tunnels running parallel to the *c* axis. The structure with the noncentrosymmetric space group can be derived by introducing slight displacements of atoms along the *c* axis in the centrosymmetric space group and both have basically the same atomic arrangement. The superstructure doubling the *c* axis of the average structure has been also reported for Sm with $x = 0.75$ (5). The space group of this structure is either $Pbn2_1$ (No. 33) or *Pbnm* (No. 62) (5). Recent reinvestigations of the solid solutions for R = Sm suggested the presence of a superstructure even for $x = 0.5$ and 0.71 (6, 7). If the structure belongs to the centrosymmetric space group *Pbnm*, there should be five crystallographically independent tetragonal tunnel sites [designated by using symbols $A_1(1)$ to $A_1(5)$] and two pentagonal tunnel sites [$A_2(1)$ and $A_2(2)$] in a unit cell. However, distributions of cations and vacancies over these seven crystallographic sites have not yet been determined.

In the $Ba_{6-3x}Sm_{8+2x}Ti_{18}O_{54}$ system, Sm is expected to be located in the perovskite-like tetragonal cavity (A_1 site) and larger Ba in the pentagonal cavity (A_2 site): a scheme of cation distribution in this system has been proposed as

$$(Sm_{8+2x}\,Ba_{2-3x}\square_x)\,[Ba_4]\,Ti_{18}O_{54} \quad (x < 2/3)$$
$$(Sm_{8+2x}\square_x)\,[Ba_{6-3x}\square_{3x-2}]\,Ti_{18}O_{54}\ (x \geq 2/3), \qquad [1]$$

where parentheses and square brackets designate A_1 and A_2 sites, respectively, and open squares designate vacancy (8). As can be seen in Eq. [1], this system has a distinctive point at $x = 2/3$ with respect to cation distribution. Substitution of Sm with Ba at the A_1 site in $x < 2/3$ and the formation of vacancy at the A_2 site in $x > 2/3$ have been

[1] To whom correspondence should be addressed.

0022-4596/99 $30.00

ascribed to the occurrence of nonlinear change in dielectric properties at its best with $x = 0.6$ (8).

In the present study, the structures of title compounds were analyzed in order to determine the distribution of cations and vacancies over tetragonal and pentagonal tunnel sites. The relationship between the physical property and the modulated local lattice distortion of the framework is discussed.

EXPERIMENTAL

Specimens

Pale-yellow sintered materials of $Ba_{6-3x}Sm_{8+2x}Ti_{18}O_{54}$ with $x = 0.3$, 0.5, 0.67, and 0.71 (hereafter abbreviated as BST30, BST50, BST67, and BST71, respectively) were synthesized by solid-state reaction of high-purity reagent chemicals of $BaCO_3$ (99.7%), TiO_2 (99.9%), and Sm_2O_3 (99.9%) mixed to attain desired compositions. They were ground into powders and used in the following experiments. Scanning-electron microscopic observations showed that individual particles had no apparent morphology corresponding to crystal habit. See Ohsato *et al.* (3) for more details.

Intensity Measurement

Powder diffraction experiments using synchrotron radiation were performed with a multiple-detector-system (MDS) (9) at the BL–4B_2 experimental station in the Photon Factory, Tsukuba. Diffracted intensities were measured with two wavelengths of 1.2 and 1.6 Å (1.54 Å for BST67) at each specimen. The wavelength calibration for monochromatic beam were made by using XANES spectra of Fe, Ni, Au, Zn, and Zr foils, and derived wavelengths were further confirmed using 10 peak positions of the NIST SRM 640b Si powder. Intensity measurements were performed at room temperature in asymmetric 2θ step scan mode at a fixed incident angle of 8° (10). A step scan technique was used at a step width of 0.005° in the 2θ-range from 20° to 80° for $\lambda = 1.2$ Å, 0.005° in the 2θ-range from 20° to 100° for $\lambda = 1.54$ Å, and 0.004° in the 2θ-range from 20° to 100° for $\lambda = 1.6$ Å.

STRUCTURE ANALYSIS

Space-Group Assignment and Rietveld Refinements

Observed diffraction patterns were resolved into individual peaks using the computer program WPPF for the whole-powder-pattern-decomposition method (11). These peaks could be indexed by assuming an orthorhombic cell ($a \approx 12$ Å, $b \approx 22$ Å and $c \approx 8$ Å, $Z = 2$) with the doubled c axis length of the reported basic cell (2). Observed systematic absences of reflections were consistent with those assigned by space groups $Pbn2_1$ and $Pbnm$. No further unindexed reflection could be observed. Parts of the profile fitting results are shown in Fig. 1.

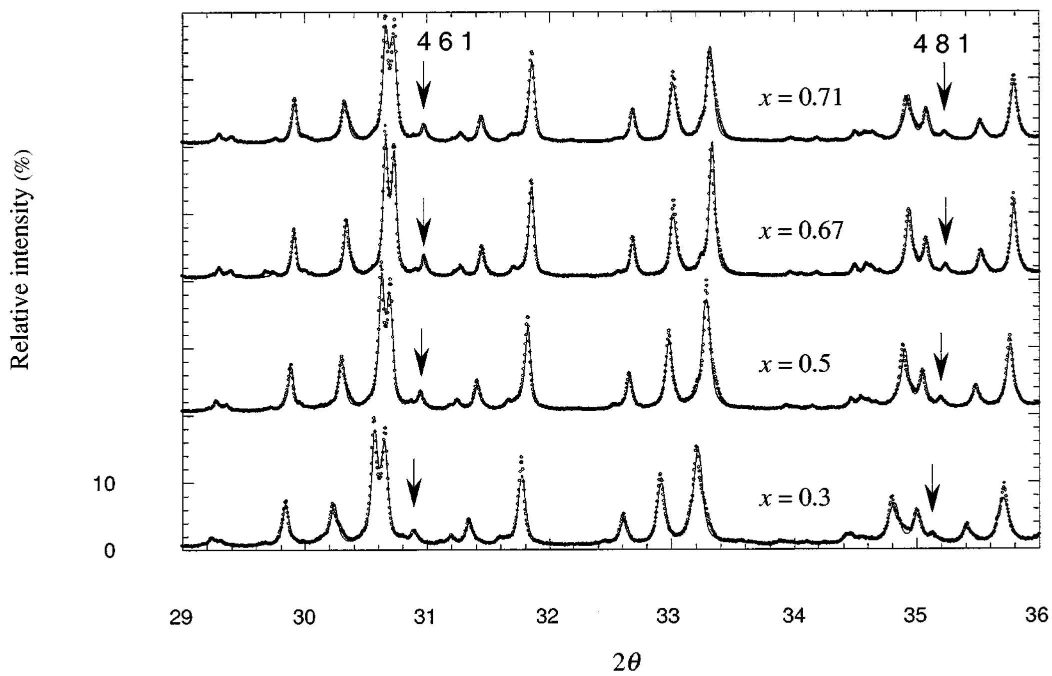

FIG. 1. Powder diffraction patterns of the $Ba_{6-3x}Sm_{8+2x}Ti_{18}O_{54}$ at $\lambda = 1.2$ Å (detail). Dots, observations; solid lines, profiles calculated by program WPPF for the whole-powder-pattern-decomposition. Vertical arrows with indices point to superstructure reflections.

Structure parameters were refined by the Rietveld method using the latest version of the computer program PFLS (12) on the assumption of the centrosymmetric space group *Pbnm*, which follows from successful single crystal structure refinements by (6, 7). In the first, profile parameters were varied. They were a scale factor, parameters of the fifth-degree polynomial background function, the unit cell, the peak-shift correction for 2θ-zero point, the pseudo-Voigt function (13), the Caglioti *et al.* formula (14), the correction for preferred orientation (15), and overall temperature parameter. After obtaining their convergence, structural parameters were varied. The structure has three types of cation sites, which are designated by using symbols Ti, A_1, and A_2 for TiO_6 octahedral sites, tetragonal tunnel sites, and pentagonal tunnel sites, respectively. Since there was parameter correlation between the thermal displacement parameters and site occupancy parameters, atoms were placed into groups of four in refining thermal displacement parameters. One group consists of Ti atoms, the second Ba/Sm atoms at the A_1 sites, the third Ba atoms at the A_2 sites, and the fourth oxygen atoms. Common thermal displacement parameters were assigned to respective groups. The Ti and oxygen sites were assumed to be fully occupied. Refinements of site occupancy parameters for the A_1 and A_2 sites will be described in next sections.

In these refinements, the weight function $w_i = 1/Y^e_{oi}$ (Y_{oi} = observed profile intensity and e is the adjustable parameter) was optimized so as to obtain a unimodal distribution of weighted residuals (16). All the atoms were assumed to be fully ionized. Scattering factors for Ti^{4+}, Ba^{2+}, and Sm^{3+} were taken from (17) and that for O^{2-} from (18). Anomalous dispersion terms at particular wavelengths were taken from (19). The constraint by the chemical composition was applied except as noted. Initial positional parameters for the refinement were taken from (6) for BST71. Other refinement conditions are given in Table 1. Refined unit cell parameters are given in Table 2.

TABLE 1
Conditions for Rietveld Structure Refinement for $Ba_{6-x}Sm_{8+2x}Ti_{18}O_{54}$

Space group	*Pbnm* (No. 62), $Z = 2$			
Profile shape	Split-type pseudo-Voigt function			
Background	5th-degree polynomial function			
Peak shift	2θ-zero point			
Preferred orientation function	Symmetrized harmonics expansion with five coefficients			
Weighting scheme	$w_i = 1/Y^e_{oi}$			
$x =$	0.3	0.5	0.67	0.71
	$\lambda = 1.60$ Å			
2θ Range analyzed (°)	$20 \le 2\theta \le 100$			
No. observations	20001	20001	16001[a]	20001
No. of flections	1051	1049	1164[a]	1046
Parameters refined (final)	101	102	102	104
e in weight function	1.8	1.8	1.4	1.6
R_p	0.11	0.09	0.12	0.10
R_{wp}	0.15	0.13	0.18	0.14
	$\lambda = 1.20$ Å			
2θ Range analyzed (°)	$20 \le 2\theta \le 80$			
No. of observations	12001	12001	12001	12001
No. of reflections	1432	1423	1417	1415
Parameters refined (final)	100	100	103	104
e in weight function	2.3	2.4	2.2	2.2
R_p	0.08	0.07	0.08	0.07
R_{wp}	0.09	0.08	0.09	0.08

[a]Data measured at step width of 0.005° and $\lambda = 1.54$ (Å), see text.

Site Occupancy Refinements for BST30 and BST50

Samples of BST30 and BST50 have 5.1 and 4.5 Ba atoms over the four A_2 sites, respectively. Thus these excess Ba were expected to coexist with Sm at the A_1 sites. The present samples will have also a certain amount of cation vacancy at the A_1 sites. Therefore, we have tried to determine the distribution of vacancies over these A_1 sites first.

If the structure is centrosymmetric, an imaginary part of the dispersion term will have a minor contribution to the structure factor. On the other hand, a sum of two real parts, Thomson scattering factor and a real part of the anomalous scattering factor, for Sm will become similar to that for Ba when the intensity data measured with the wavelength of 1.6 Å are used. In this case, two kinds of different atoms can be treated as one kind of atom, when only the total scattering powers are taken into account, in the determination of vacancies at the A_1 sites using a 1.6-Å data set. In the least-squares calculations at this stage, the same occupancy ratio of Ba/Sm was assigned to the atoms at the five A_1 sites. The occupancy parameters for the $A_1(5)$ site became slightly larger than 1, and thus it was kept fixed at 1 in further calculation. Parameters were converged after several iterations of the least-squares cycles. A result of the determination of vacancy distribution is presented in Table 3. It showed that the vacancies are distributed over the $A_1(1)$ sites by 11 to 17% and over the $A_1(3)$ and $A_1(4)$ sites in small amounts. The R_p and R_{wp} factors were 0.11 and 0.15 for BST30 and 0.09 and 0.13 for BST50, respectively, at this stage.

TABLE 2
The Unit-Cell Parameters for $Ba_{6-3x}Sm_{8+2x}Ti_{18}O_{54}$

Composition, x	0.3	0.5	0.67	0.71
Cell dimensions (Å)				
$a =$	12.1715(5)	12.1568(1)	12.1472(1)	12.1452(1)
$b =$	22.3772(3)	22.3253(2)	22.2972(2)	22.3029(2)
$c =$	7.67523(9)	7.66301(7)	7.65338(6)	7.65007(6)
Volume (Å^3)	2090.45(4)	2079.78(3)	2072.91(3)	2072.20(3)

TABLE 3
Site Occupancies and Their E.s.d.s for Tetragonal and Pentagonal Sites

Site	Atom	$x = 0.3$	$x = 0.5$	$x = 0.67$	$x = 0.71$
		$\lambda = 1.6$ (Å)			
$A_1(1)$		0.89(1)	0.833(8)		
$A_1(2)$		1.00(1)	0.994(8)		
$A_1(3)$		0.989(8)	0.954(7)		
$A_1(4)$		0.97(1)	0.970(9)		
$A_1(5)$		1	1		
		$\lambda = 1.2$ (Å)			
$A_1(1)$	Sm	0.68(6)	0.72(4)	0.791(6)	0.803(5)
	Ba	0.21	0.12		
$A_1(2)$	Sm	1.00[a]	0.994[a]	0.982(7)	0.989(5)
$A_1(3)$	Sm	0.65(4)	0.82(4)	0.910(6)	0.919(5)
	Ba	0.34	0.13		
$A_1(4)$	Sm	0.97[a]	0.970[a]	0.993(7)	0.990(6)
$A_1(5)$	Sm	1[a]	1[a]	0.991(6)	1
$A_2(1)$	Ba	1	1	1	0.988(7)
$A_2(2)$	Ba	1	1	1	0.952(7)

[a]Obtained by refinements at $\lambda = 1.6$ Å

After fixing the amount of vacancy, the distributions of Sm and Ba over the five A_1 sites could be determined by using intensity data measured with the wavelength of 1.2 Å. The occupancy parameter of Ba at the $A_1(2)$, $A_1(4)$, and $A_1(5)$ sites became slightly negative, and then they were kept fixed at zero in further calculation. All parameters converged and the final R_p and R_{wp} factors were 0.08 and 0.09 for BST30 and 0.07 and 0.08 for BST50, respectively. Site occupancy parameters, thus obtained, are presented in Table 3. Other positional parameters and thermal displacement parameters are given in Table 4. Selected interatomic distances are given in Tables 5 and 6. A fitting result in Rietveld refinement for BST30 is given in Fig. 2.

Site Occupancy Refinement for BST67 and BST71

Samples of BST71 have vacancies at both A_1 and A_2 sites and samples of BST67 have vacancies at A_1 sites. In the first, the site occupancy parameters of Sm and Ba at respective sites were varied independently. In this case, the constraint by the chemical composition was not applied. Two sets of refinements using the two wavelength data sets for 1.2 and 1.6 Å (1.54 Å for BST67) resulted in virtually the same result, indicating no exchange of Ba at the A_2 sites with Sm atoms at the A_1 site and vice versa.

Second, the site occupancy parameters were refined. The parameters became larger than 1 for the $A_1(5)$ site in BST71. Thus it was kept fixed at 1 in further calculation. The final R_p and R_{wp} factors after the least-squares calculations were 0.08 and 0.09 for BST67 and 0.07 and 0.08 for BST71,

TABLE 4
Refined Positional and Isotropic Thermal Displacement Parameters and Their E.s.d.s for $Ba_{6-3x}Sm_{8+2x}Ti_{18}O_{54}$

	x	y	z	B_{iso} (Å^2)[a]
	$Ba_{5.1}Sm_{8.6}Ti_{18}O_{54}$ (BST30 $x = 0.3$)			
Ti(1)	0.0	0.0	0.0	0.55(4)
Ti(2)	0.1994(4)	0.4336(2)	0.001(1)	0.55
Ti(3)	0.3977(4)	0.1069(2)	− 0.000(1)	0.55
Ti(4)	0.1187(4)	0.1641(2)	− 0.009(1)	0.55
Ti(5)	0.3400(4)	0.2604(2)	− 0.003(1)	0.55
$A_1(1)$	0.1926(2)	0.0462(1)	1/4	0.59(3)
$A_1(2)$	0.7053(2)	0.4486(1)	1/4	0.59
$A_1(3)$	1.0008(3)	0.4948(1)	1/4	0.59
$A_1(4)$	0.4050(3)	0.3776(1)	1/4	0.59
$A_1(5)$	0.9091(3)	0.1234(1)	1/4	0.59
$A_2(1)$	0.0866(2)	0.3013(1)	1/4	0.65(4)
$A_2(2)$	0.5966(2)	0.1870(1)	1/4	0.65
O(1)	0.093(2)	0.167(1)	1/4	0.55(9)
O(2)	0.595(2)	0.363(1)	1/4	0.55
O(3)	0.423(1)	0.1932(6)	0.013(4)	0.55
O(4)	0.688(1)	0.2621(6)	− 0.016(3)	0.55
O(5)	0.336(2)	0.275(1)	1/4	0.55
O(6)	0.811(2)	0.222(1)	1/4	0.55
O(7)	0.377(1)	0.0174(6)	0.003(3)	0.55
O(8)	0.215(2)	0.443(1)	1/4	0.55
O(9)	0.679(2)	0.057(1)	1/4	0.55
O(10)	0.242(1)	0.1095(6)	0.028(2)	0.55
O(11)	0.479(2)	0.482(1)	1/4	0.55
O(12)	0.039(1)	0.0808(7)	0.060(2)	0.55
O(13)	0.759(1)	0.1409(7)	0.037(2)	0.55
O(14)	0.848(1)	0.0197(7)	0.051(2)	0.55
O(15)	0.055(1)	0.4071(6)	0.045(2)	0.55
O(16)	0.457(1)	0.3184(6)	0.021(3)	0.55
O(17)	0.432(2)	0.0993(9)	1/4	0.55
O(18)	0.877(2)	0.409(1)	1/4	0.55
	$Ba_{4.5}Sm_{9.0}Ti_{18}O_{54}$ (BST50 $x = 0.5$)			
Ti(1)	0.0	0.0	0.0	0.53(3)
Ti(2)	0.1994(3)	0.4339(1)	0.0042(8)	0.53
Ti(3)	0.3980(3)	0.1068(1)	0.0078(7)	0.53
Ti(4)	0.1176(3)	0.1632(2)	0.0002(9)	0.53
Ti(5)	0.3397(3)	0.2612(1)	0.0002(9)	0.53
$A_1(1)$	0.1930(2)	0.0452(1)	1/4	0.63(3)
$A_1(2)$	0.7047(2)	0.44887(8)	1/4	0.63
$A_1(3)$	0.9999(2)	0.4946(1)	1/4	0.63
$A_1(4)$	0.4043(2)	0.37745(9)	1/4	0.63
$A_1(5)$	0.9095(2)	0.12405(8)	1/4	0.63
$A_2(1)$	0.0851(2)	0.30026(9)	1/4	0.54(2)
$A_2(2)$	0.5957(2)	0.18673(8)	1/4	0.54
O(1)	0.104(2)	0.1746(9)	1/4	1.11(8)
O(2)	0.592(2)	0.3578(9)	1/4	1.11
O(3)	0.421(1)	0.1934(5)	0.005(3)	1.11
O(4)	0.6862(9)	0.2638(6)	0.005(3)	1.11
O(5)	0.311(2)	0.2751(9)	1/4	1.11
O(6)	0.845(2)	0.2182(9)	1/4	1.11
O(7)	0.380(1)	0.0161(5)	− 0.004(2)	1.11
O(8)	0.225(2)	0.4424(8)	1/4	1.11
O(9)	0.675(2)	0.0524(9)	1/4	1.11
O(10)	0.244(1)	0.1106(5)	0.013(2)	1.11
O(11)	0.478(2)	0.4839(8)	1/4	1.11
O(12)	0.037(1)	0.0809(6)	0.049(2)	1.11

TABLE 4—*Continued*

	x	y	z	B_{iso} (Å^2)[a]
	$Ba_{4.5}Sm_{9.0}Ti_{18}O_{54}$ (BST50 x = 0.5)			
O(13)	0.762(1)	0.1380(5)	0.029(2)	1.11
O(14)	0.845(1)	0.0194(6)	0.047(2)	1.11
O(15)	0.058(1)	0.4062(5)	0.045(2)	1.11
O(16)	0.460(1)	0.3172(5)	0.018(3)	1.11
O(17)	0.428(2)	0.1010(8)	1/4	1.11
O(18)	0.878(2)	0.4058(9)	1/4	1.11
	$Ba_{3.99}Sm_{9.34}Ti_{18}O_{54}$ (BST67 x = 0.67)			
Ti(1)	0.0	0.0	0.0	0.41(4)
Ti(2)	0.1998(3)	0.4339(2)	0.0050(8)	0.41
Ti(3)	0.3971(3)	0.1062(1)	0.0108(7)	0.41
Ti(4)	0.1168(3)	0.1634(2)	0.0012(8)	0.41
Ti(5)	0.3393(3)	0.2618(2)	0.0025(9)	0.41
A_1(1)	0.1935(2)	0.0446(1)	1/4	0.65(3)
A_1(2)	0.7047(2)	0.44894(9)	1/4	0.65
A_1(3)	0.9991(2)	0.4944(1)	1/4	0.65
A_1(4)	0.4046(2)	0.37708(9)	1/4	0.65
A_1(5)	0.9089(2)	0.12402(9)	1/4	0.65
A_2(1)	0.0846(2)	0.29986(9)	1/4	0.55(4)
A_2(2)	0.5960(2)	0.18715(9)	1/4	0.55
O(1)	0.102(2)	0.1770(9)	1/4	1.3(1)
O(2)	0.595(2)	0.3565(9)	1/4	1.3
O(3)	0.419(1)	0.1951(6)	0.007(3)	1.3
O(4)	0.687(1)	0.2630(6)	0.014(3)	1.3
O(5)	0.309(2)	0.2734(9)	1/4	1.3
O(6)	0.845(2)	0.215(1)	1/4	1.3
O(7)	0.378(1)	0.0151(6)	0.012(2)	1.3
O(8)	0.227(2)	0.4442(9)	1/4	1.3
O(9)	0.671(2)	0.054(1)	1/4	1.3
O(10)	0.242(1)	0.1113(6)	0.016(2)	1.3
O(11)	0.476(2)	0.4841(9)	1/4	1.3
O(12)	0.037(1)	0.0818(6)	0.042(2)	1.3
O(13)	0.767(1)	0.1378(6)	0.026(2)	1.3
O(14)	0.849(1)	0.0214(7)	0.047(2)	1.3
O(15)	0.059(1)	0.4093(6)	0.047(2)	1.3
O(16)	0.461(1)	0.3154(6)	0.013(3)	1.3
O(17)	0.427(2)	0.1016(8)	1/4	1.3
O(18)	0.878(2)	0.413(1)	1/4	1.3
	$Ba_{3.87}Sm_{9.42}Ti_{18}O_{54}$ (BST71 x = 0.71)			
Ti(1)	0.0	0.0	0.0	0.71(3)
Ti(2)	0.1992(3)	0.4343(1)	0.0025(7)	0.71
Ti(3)	0.3981(3)	0.1069(1)	0.0080(7)	0.71
Ti(4)	0.1172(3)	0.1630(2)	0.0010(8)	0.71
Ti(5)	0.3388(3)	0.2616(2)	0.0006(8)	0.71
A_1(1)	0.1936(2)	0.0449(1)	1/4	0.63(2)
A_1(2)	0.7047(2)	0.44900(8)	1/4	0.63
A_1(3)	0.9988(2)	0.4942(1)	1/4	0.63
A_1(4)	0.4042(2)	0.37696(8)	1/4	0.63
A_1(5)	0.9095(2)	0.12400(8)	1/4	0.63
A_2(1)	0.0845(2)	0.30012(9)	1/4	0.54(4)
A_2(2)	0.5958(2)	0.18716(9)	1/4	0.54
O(1)	0.100(2)	0.1766(9)	1/4	1.41(8)
O(2)	0.591(2)	0.3584(9)	1/4	1.41
O(3)	0.419(1)	0.1929(6)	0.006(3)	1.41
O(4)	0.6871(9)	0.2637(6)	0.012(2)	1.41
O(5)	0.309(2)	0.2760(9)	1/4	1.41
O(6)	0.853(2)	0.2160(9)	1/4	1.41
O(7)	0.3752(9)	0.0161(5)	0.003(2)	1.41
O(8)	0.228(2)	0.4424(8)	1/4	1.41
O(9)	0.670(2)	0.0532(9)	1/4	1.41
O(10)	0.242(1)	0.1089(6)	0.019(2)	1.41
O(11)	0.477(2)	0.4840(8)	1/4	1.41
O(12)	0.037(1)	0.0807(6)	0.042(2)	1.41
O(13)	0.767(1)	0.1388(5)	0.026(2)	1.41
O(14)	0.848(1)	0.0195(6)	0.045(2)	1.41
O(15)	0.058(1)	0.4071(5)	0.049(2)	1.41
O(16)	0.461(1)	0.3170(5)	0.011(3)	1.41
O(17)	0.426(2)	0.1012(8)	1/4	1.41
O(18)	0.880(2)	0.4077(9)	1/4	1.41

[a]Common B_{iso}s were used for each Ti-, A_1-, A_2-, and O- site atoms.

respectively. Final atomic parameters are given in Tables 3 and 4. Selected interatomic distances are given in Tables 5 and 6.

TABLE 5
Selected Interatomic Distances (Å) and Their E.s.d.s at the TiO_6 Octahedra of $Ba_{6-3x}Sm_{8+2x}Ti_{18}0_{54}$

	$x = 0.3$	$x = 0.5$	$x = 0.67$	$x = 0.71$
Ti(1)–O(11) 2×	1.976(5)	1.967(4)	1.967(5)	1.965(4)
Ti(1)–O(12) 2×	1.93(2)	1.90(1)	1.91(1)	1.88(1)
Ti(1)–O(13) 2×	1.94(2)	1.96(1)	1.93(1)	1.92(1)
Mean value	1.95(1)	1.94(1)	1.94(1)	1.92(1)
Ti(2)–O(7)	2.10(1)	2.07(1)	2.04(1)	2.03(1)
Ti(2)–O(8)	1.933(9)	1.920(7)	1.917(7)	1.933(7)
Ti(2)–O(9)	1.952(9)	1.993(8)	2.000(7)	1.984(7)
Ti(2)–O(13)	1.84(2)	1.79(1)	1.81(1)	1.84(1)
Ti(2)–O(14)	2.13(2)	2.10(1)	2.10(1)	2.11(1)
Ti(2)–O(15)	1.88(2)	1.85(1)	1.83(1)	1.86(1)
Mean value	1.97(1)	1.95(1)	1.95(1)	1.96(1)
Ti(3)–O(3)	1.96(1)	1.96(1)	2.00(1)	1.93(1)
Ti(3)–O(7)	2.02(1)	2.04(1)	2.05(1)	2.05(1)
Ti(3)–O(10)	1.91(2)	1.87(1)	1.89(1)	1.90(1)
Ti(3)–O(15)	1.97(2)	2.01(1)	2.04(1)	2.01(1)
Ti(3)–O(17)	1.973(9)	1.895(7)	1.869(7)	1.886(6)
Ti(3)–O(18)	1.964(9)	2.011(7)	2.053(7)	2.013(7)
Mean value	1.97(1)	1.96(1)	1.98(1)	1.96(1)
Ti(4)–O(1)	2.011(9)	1.939(7)	1.937(8)	1.939(7)
Ti(4)–O(2)	1.97(1)	1.997(9)	1.991(9)	2.005(9)
Ti(4)–O(3)	1.86(1)	1.83(1)	1.85(1)	1.84(1)
Ti(4)–O(10)	1.96(2)	1.94(1)	1.91(1)	1.94(1)
Ti(4)–O(12)	2.17(2)	2.12(1)	2.09(1)	2.10(1)
Ti(4)–O(16)	2.01(1)	1.97(1)	1.95(1)	1.95(1)
Mean value	2.00(1)	1.96(1)	1.95(1)	1.96(1)
Ti(5)–O(3)	1.82(1)	1.81(1)	1.78(1)	1.81(1)
Ti(5)–O(4)	1.92(1)	1.95(1)	1.94(1)	1.93(1)
Ti(5)–O(5)	1.97(1)	1.970(9)	1.946(8)	1.968(8)
Ti(5)–O(6)	1.96(1)	1.973(9)	2.004(9)	1.989(8)
Ti(5)–O(13)	2.43(2)	2.45(1)	2.42(1)	2.40(1)
Ti(5)–O(16)	1.94(1)	1.93(1)	1.91(1)	1.94(1)
Mean value	2.01(1)	2.01(1)	2.00(1)	2.01(1)

TABLE 6
Selected Interatomic Distances (Å) and Their E.s.d.s at the Tetragonal and Pentagonal Sites of $Ba_{6-3x}Sm_{8+2x}Ti_{18}0_{54}$

	$x = 0.3$	$x = 0.5$	$x = 0.67$	$x = 0.71$
$A_1(1)$–O(1)	2.96(2)	3.09(2)	3.16(2)	3.15(2)
$A_1(1)$–O(7) 2×	3.01(2)	3.06(1)	2.96(1)	2.97(1)
$A_1(1)$–O(8)	2.57(2)	2.50(2)	2.44(2)	2.48(2)
$A_1(1)$–O(10) 2×	2.29(2)	2.41(2)	2.40(2)	2.35(2)
$A_1(1)$–O(11)	2.53(2)	2.49(2)	2.47(2)	2.48(2)
$A_1(1)$–O(12) 2×	2.49(2)	2.57(1)	2.62(1)	2.61(1)
$A_1(1)$–O(14) 2×	2.78(2)	2.74(1)	2.75(2)	2.72(1)
$A_1(1)$–O(17)	3.15(2)	3.12(2)	3.11(2)	3.08(2)
Mean value	2.70(2)	2.73(1)	2.72(1)	2.71(1)
$A_1(2)$–O(2)	2.34(2)	2.45(2)	2.46(2)	2.45(2)
$A_1(2)$–O(7) 2×	2.95(2)	2.95(1)	3.01(2)	2.94(1)
$A_1(2)$–O(9)	2.80(2)	2.73(2)	2.79(2)	2.78(2)
$A_1(2)$–O(10)2×	2.54(2)	2.46(2)	2.48(2)	2.47(2)
$A_1(2)$–O(11)	2.86(2)	2.86(2)	2.88(2)	2.87(2)
$A_1(2)$–O(12) 2×	3.19(2)	3.14(1)	3.10(1)	3.10(1)
$A_1(2)$–O(14) 2×	2.30(2)	2.29(1)	2.33(2)	2.32(1)
$A_1(2)$–O(18)	2.28(2)	2.32(2)	2.26(2)	2.31(2)
Mean value	2.68(2)	2.67(2)	2.69(2)	2.67(2)
$A_1(3)$–O(7) 2×	2.46(2)	2.48(2)	2.40(2)	2.48(2)
$A_1(3)$–O(7)′ 2×	2.47(2)	2.40(2)	2.50(2)	2.46(2)
$A_1(3)$–O(8)	2.85(3)	2.98(2)	2.98(2)	3.01(2)
$A_1(3)$–O(9)	2.60(2)	2.49(2)	2.46(2)	2.44(2)
$A_1(3)$–O(15) 2×	2.60(1)	2.62(1)	2.56(1)	2.58(1)
$A_1(3)$–O(15)′ 2×	3.22(2)	3.24(1)	3.21(1)	3.25(1)
$A_1(3)$–O(17)	2.48(2)	2.53(2)	2.55(2)	2.56(2)
$A_1(3)$–O(18)	2.45(2)	2.48(2)	2.34(2)	2.41(2)
Mean value	2.66(2)	2.66(2)	2.64(2)	2.66(2)
$A_1(4)$–O(2)	2.33(3)	2.33(2)	2.36(2)	2.30(2)
$A_1(4)$–O(5)	2.44(3)	2.55(2)	2.59(2)	2.53(2)
$A_1(4)$–O(8)	2.74(3)	2.62(2)	2.63(2)	2.59(2)
$A_1(4)$–O(11)	2.51(2)	2.54(2)	2.54(2)	2.55(2)
$A_1(4)$–O(12) 2×	3.03(2)	2.95(1)	2.90(1)	2.91(1)
$A_1(4)$–O(13) 2×	2.86(2)	2.77(2)	2.71(2)	2.71(2)
$A_1(4)$–O(14) 2×	3.33(2)	3.32(1)	3.28(2)	3.30(1)
$A_1(1)$–O(16) 2×	2.29(2)	2.33(2)	2.38(2)	2.37(2)
Mean value	2.75(2)	2.73(2)	2.72(2)	2.72(2)
$A_1(5)$–O(1)	2.43(3)	2.62(2)	2.63(2)	2.60(2)
$A_1(5)$–O(6)	2.52(2)	2.24(2)	2.16(2)	2.16(2)
$A_1(5)$–O(9)	3.16(2)	3.27(2)	3.28(2)	3.31(2)
$A_1(5)$–O(11)	3.44(2)	3.41(2)	3.42(2)	3.41(2)
$A_1(5)$–O(12) 2×	2.35(2)	2.39(1)	2.41(1)	2.42(1)
$A_1(5)$–O(13) 2×	2.48(2)	2.49(2)	2.45(2)	2.46(1)
$A_1(5)$–O(14) 2×	2.87(2)	2.91(1)	2.86(1)	2.91(2)
$A_1(5)$–O(16) 2×	2.52(2)	2.51(2)	2.50(2)	2.47(2)
Mean value	2.67(2)	2.68(2)	2.66(2)	2.67(2)
$A_2(1)$–O(1)	3.02(2)	2.81(2)	2.75(2)	2.76(2)
$A_2(1)$–O(3) 2×	2.84(2)	2.79(2)	2.81(2)	2.81(2)
$A_2(1)$–O(4) 2×	2.60(2)	2.72(2)	2.75(2)	2.75(2)
$A_2(1)$–O(5)	3.09(3)	2.80(2)	2.79(2)	2.78(2)
$A_2(1)$–O(6)	3.79(2)	3.44(2)	3.47(2)	3.37(2)
$A_2(1)$–O(8)	3.53(2)	3.60(2)	3.65(2)	3.62(2)
$A_2(1)$–O(13) 2×	3.30(2)	3.33(1)	3.36(2)	3.35(1)
$A_2(1)$–O(15) 2×	2.87(1)	2.86(1)	2.91(1)	2.86(1)
$A_2(1)$–O(16) 2×	3.74(2)	3.66(2)	3.59(2)	3.61(2)
$A_2(1)$–O(18)	3.50(2)	3.45(2)	3.55(2)	3.46(2)
Mean value	3.18(2)	3.12(2)	3.14(2)	3.12(2)
$A_2(2)$–O(2)	3.94(2)	3.81(2)	3.78(2)	3.82(2)
$A_2(2)$–O(3) 2×	2.79(2)	2.83(2)	2.85(2)	2.85(2)
$A_2(2)$–O(4) 2×	2.87(2)	2.77(2)	2.71(2)	2.73(2)
$A_2(2)$–O(5)	3.74(3)	3.99(2)	3.98(2)	4.00(2)
$A_2(2)$–O(6)	2.73(2)	3.11(2)	3.09(2)	3.20(2)
$A_2(2)$–O(9)	3.07(3)	3.15(2)	3.11(2)	3.12(2)
$A_2(2)$–O(13) 2×	2.77(2)	2.85(1)	2.91(2)	2.90(1)
$A_2(2)$–O(15) 2×	3.13(2)	3.10(1)	3.16(1)	3.14(1)
$A_2(2)$–O(16) 2×	3.83(2)	3.79(1)	3.76(2)	3.79(1)
$A_2(2)$–O(17)	2.80(2)	2.80(2)	2.80(2)	2.82(2)
Mean value	3.14(2)	3.17(2)	3.17(2)	3.19(2)

RESULTS AND DISCUSSION

Cation Distribution and Interatomic Distances

A projection of the crystal structure of BST30 on a (0 0 1) plane is shown in Fig. 3. As has been described above, present solid solutions have TiO_6-framework structures with the five tetragonal and two pentagonal tunnels running parallel to the c axis.

Results of the site occupancy refinements given in Table 3 showed that two of five tetragonal A_1 sites [$A_1(1)$ and $A_1(3)$] accommodate Ba in BST30 and BST50. Most of cation vacancies were also found at these two $A_1(1)$ and $A_1(3)$ sites in the samples examined. In particular, the $A_1(1)$ site commonly had smaller site occupancy than the others, and more than 2/3 of total vacancies are concentrated at this site. The $A_1(4)$ site have a little vacancy and the other two tetragonal sites [$A_1(2)$ and $A_1(5)$] are virtually fully occupied by Sm. The total occupancies of Ba and Sm at the $A_1(1)$ and $A_1(3)$ sites have their minima with $x = 0.67$, as expected from Eq. [1]. These minima are caused by (i) decreasing amount of Sm with decreasing x and (ii) substitution of Ba at these sites in $x < 0.67$. The $A_1(1)$ and $A_1(2)$ sites are crystallographically identical in the average structure. Therefore, this observation suggests that the formation of superstructure is due to the ordering of vacancy in the average structure. With $x = 0.71$, cation vacancy was also found at $A_2(2)$ site.

TABLE 7
Selected Bending Angles (°) and Their E.s.d.s of the TiO_6 Octahedra Joining along the c Axis

	$x = 0.3$	$x = 0.5$	$x = 0.67$	$x = 0.71$
O(11)–O(11)′–O(11)	152.3(6)	153.8(5)	153.3(6)	153.5(6)
O(9)–O(8)–O(9)	167.1(7)	161.6(6)	160.0(6)	159.1(6)
O(18)–O(17)–O(18)	159.6(7)	161.4(6)	160.1(6)	162.4(6)
O(2)–O(1)–O(2)	160.4(7)	158.2(6)	157.8(6)	156.7(6)
O(6)–O(5)–O(6)	170.9(7)	166.8(6)	164.7(7)	163.2(6)
Mean value	162.1(7)	160.4(6)	159.2(6)	159.0(6)

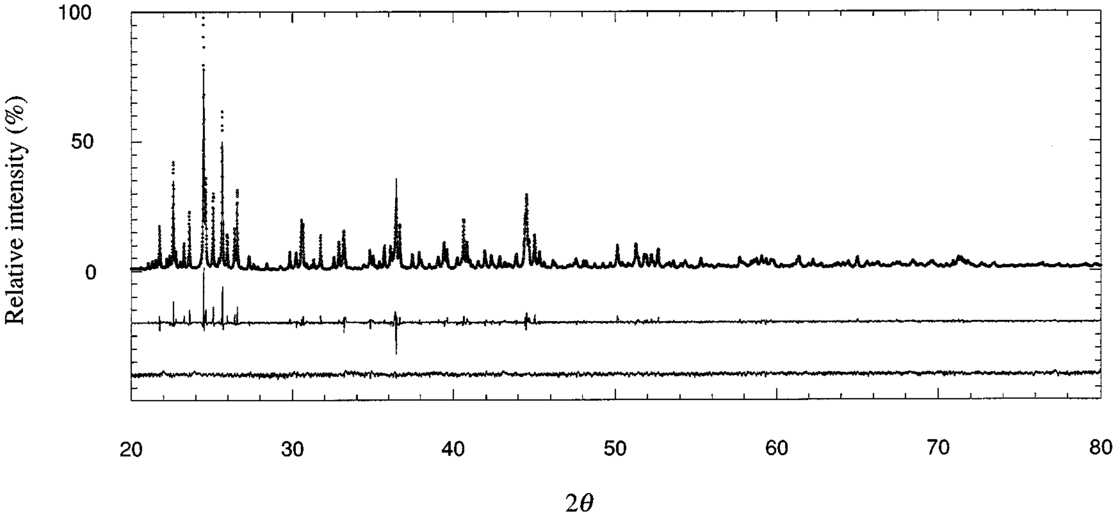

FIG. 2. Powder diffraction pattern of $Ba_{5.1}Sm_{8.6}Ti_{18}O_{54}$ and its fitting results by Rietveld refinement. (Top) Observations (dots) and calculated profile (solid line); (middle) difference between observations and calculated profile; (bottom) weighted difference (×5).

As given in Table 6, $A_2(1)$–O and $A_2(2)$–O bond lengths remain unchanged. In spite of the substitution of Ba, averaged $A_1(3)$–O bond lengths also remain unchanged. The Ba–O distance calculated by the bond-valence scheme is 2.66 Å (20), which is fairly close to, or slightly smaller than, the observed A_1–O distances. In contrast with that, the $A_1(4)$–O bond lengths appear to be steadily increased with decreasing occupancy at the $A_1(4)$ site. These observations suggest that these tetragonal cavities formed by 2 × 2 perovskite-like blocks have an enough room for larger Ba and partial substitution of Ba has rather minor effect on A_1–O bond distances.

Lattice Deformation

The lattice modulation, which doubles the *c* axis of the basic structure, can be illustrated as zig-zag bending of TiO_6 octahedra parallel to the *c* axis (Fig. 4) (21). A bending angle of two TiO_6 octahedra running parallel to the *c* axis can be used as a measure of the lattice modulation. Observed bending angles given in Table 7 show that the mean value of these angles decreases with increasing *x*, indicating more lattice distortion with larger *x* value. The increasing amount of cation vacancy at the $A_1(1)$ site, which is equivalent to the $A_1(2)$ site in the basic structure, will force to deform the framework. Even with partial substitution of Ba for Sm, the increase of total population at the $A_1(1)$ and $A_1(3)$ sites reduces an amplitude of this lattice modulation.

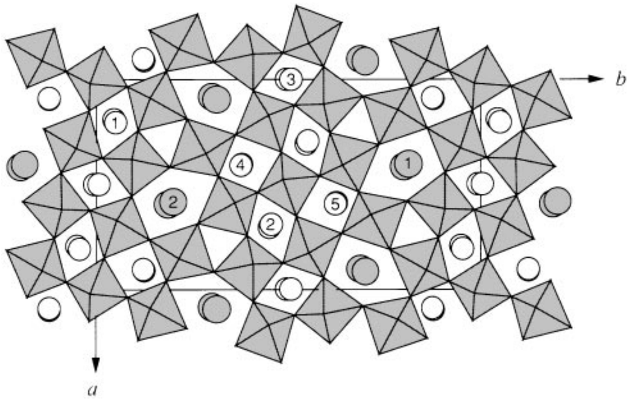

FIG. 3. TiO_6-framework structure of $Ba_{6-3x}Sm_{8+2x}Ti_{18}O_{54}$. Tetragonal and pentagonal site atoms were shown in white and shaded circles, respectively.

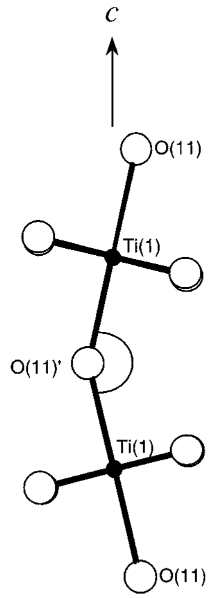

FIG. 4. Two TiO_6 octahedra sharing an apex and arrayed parallel to the *c* axis. Ti(1) is located at center of symmetry. Interatomic distance between two O(11) corresponds to the *c*-axis length of the cell.

TABLE 8
Observed Relative Intensities (%)[a] of Some Superstructure Reflections

	Intensity			
Bragg indices	$x = 0.3$	$x = 0.5$	$x = 0.67$	$x = 0.71$
4 6 1	2.8	3.7	3.9	3.8
4 8 1	1.8	2.5	2.8	2.4

[a]Intensities at $\lambda = 1.2$ Å were normalized with those of 1 2 5 reflection (most intense one).

Obtained by program WPPF for whole–powder-pattern decomposition.

Observed intensities of some superstructure reflections are presented in Table 8. In spite of the steady change of calculated superstructure intensities with x, the observed ones increased with x in $x < 0.67$ and then reduced with x from 0.67 to 0.71. This observation indicates that local lattice distortion, in addition to a long-range lattice modulation mentioned above, is possibly induced by the occupation of Ba and Sm at the same site in the composition range $x < 2/3$ and the ordering of vacancy at A_2 sites in $x > 2/3$. This observation is in accordance with the observed physical properties, particularly of the quality factor having its maximum at $x = 0.6$ (8).

ACKNOWLEDGMENTS

Authors thank Mr. M. Imaeda at Nagoya Institute of Technology for useful discussions. This study has benefited from the use of facility at Photon Factory, High Energy Accelerator Research Organization at Tsukuba, Japan.

REFERENCES

1. R. G. Matveeva, M. B. Varfolomeev, and L. S. Il'yushchenko, *Zh. Neorg. Khim.* **29,** 31 (1984). [Translation: *Russ. J. Inorg. Chem.* **29**, 17 (1984)]
2. H. Ohsato, T. Ohhashi, and T. Okuda, *Ext. Abstr. AsCA* '93 *Conf.* 14U-50, Singapore, November (1993).
3. H. Ohsato, T. Ohhashi, S. Nishigaki, T. Okuda, K. Sumiya, and S. Suzuki, *Jpn. J. Appl. Phys.* **32,** 4323 (1993).
4. H. Ohsato, T. Ohhashi, H. Kato, S. Nishigaki, and T. Okuda, *Jpn. J. Appl. Phys.* **34,** 187 (1995).
5. H. Ohsato, S. Nishigaki, and T. Okuda, *Jpn. J. Appl. Phys.* **31,** 3136 (1992).
6. H. Kato, MS thesis, Nagoya Institute of Technology, 1995.
7. M. Imaeda, MS thesis, Nagoya Institute of Technology, 1998.
8. H. Ohsato, M. Imaeda, M. Mizuta, S. Nishigaki, and T. Okuda, *Abst. Annu. Meeting Jpn. Crystallogr. Soc*, OA-02 (1997).
9. H. Toraya, H. Hibino, and K. Ohsumi, *J. Synchrotron Radiat.* **3,** 75 (1996).
10. H. Toraya, *J. Appl. Crystallogr.* **26,** 774 (1993).
11. H. Toraya, *J. Appl. Crystallogr.* **19,** 440 (1986).
12. H. Toraya and F. Marumo, *Rep. Res. Lab. Eng. Mater. Tokyo Inst. Technol.* **5**, 55 (1980).
13. H. Toraya, *J. Appl. Crystallogr.* **23,** 485 (1990).
14. G. Caglioti, A. Paoletti, and F. Ricci, *Nucl. Instrum. Methods* **3,** 223 (1958).
15. M. Järvinen, *J. Appl. Crystallogr.* **26,** 525 (1993)
16. H. Toraya, *J. Appl. Crystallogr.* **31,** 333 (1998).
17. "International Tables for X-ray Crystallography," Vol. IV. Kynoch Press, Birmingham, 1974. [Present distributor: Kluwer, Academic, Dordrecht]
18. M. Tokonami, *Acta Crystallogr.* **19,** 486 (1965).
19. S. Sasaki, KEK Report 88-14 (1989).
20. I. D. Brown and D. Altermatt, *Acta Crystallogr. Sect. B* **41,** 244 (1985).
21. T. Ohhashi, MS thesis, Nagoya Institute of Technology, 1994.